Physical and chemical properties of lunar magma

van Kan, M.

2011

Chapter 8

Trace element evolution during crystallisation and remelting of the lunar magma ocean

Mirjam van Kan Parker, Wim van Westrenen

ABSTRACT

Newly determined ilmenite-melt and orthopyroxene-melt partition coefficients are used to construct quantitative forward models of the evolution of high field strength element (HFSE, Zr, Nb, Hf, Ta, Th, U) and rare earth element (REE: Nd, Sm, Lu) concentrations during crystallisation and subsequent remelting of the Lunar Magma Ocean (LMO). Crystallisation models suggest that the initial LMO must have been enriched in these elements with respect to the bulk silicate earth. This is required to account for the trace element concentrations of KREEP samples, which are enriched in potassium, rare earth elements and phosphorus. The trace element signatures and ratios found in the low-Ti and high-Ti mare basalts can be explained by partial melting of a mixture of early-formed olivine and orthopyroxene cumulates, as long as these contain 1-3 wt% of trapped residual liquid (TRL), which fully equilibrated with the cumulates prior to remelting. The observed Nb/Ta, Zr/Hf, Sm/Nd and Lu/Hf systematics of the high-Ti basalts can be explained by mixing partial melts of early olivine and orthopyroxene cumulates with clinopyroxene and ilmenite (ratio 1:3) or with ilmenite only. The Zr/Hf, Sm/Nd and Lu/Hf ratios of low Ti-basalts are best explained by a mix of low-degree (2%) partial melts of Ol and Opx cumulates, that include a 3 wt% TRL. However, modelled Nb/Ta ratios are elevated with respect to ratios measured in the low-Ti basalts in this case, and thus dissolution of a mineral or late stage cumulate possessing subchondritic Nb/Ta ratios seems required. The subchondritic Nb/Ta ratios in lunar samples can be reproduced from an initial lunar magma ocean with a chondritic Nb/Ta ratio.

1. INTRODUCTION

The presence of a global lunar magma ocean (LMO) (e.g. Smith et al., 1970; Wood et al., 1970; Warren, 1985; Shearer and Papike, 1999; Shearer et al., 2006) directly following lunar accretion, played a critical role in the subsequent thermal and chemical evolution of the Moon. Cooling and crystallisation of the LMO are thought to have led to a chemically differentiated and stratified mantle. The general LMO crystallisation sequence is determined by the initial bulk composition of the LMO and by assumptions about the efficiency of crystal-melt segregation, can be summarised as 1) olivine; 2) orthopyroxene ± olivine; 3) olivine + clinopyroxene ± plagioclase; 4) clinopyroxene + plagioclase and 5) clinopyroxene + plagioclase + ilmenite (e.g. Taylor and Jakes, 1974; Snyder et al., 1992; Shearer and Papike, 1999; Shearer et al., 2006).

The density contrast between the relatively light plagioclase and residual melt from which it crystallised led to its buoyant rise, forming the anorthositic crust. Late crystallisation of a titanium-rich cumulate layer, the so-called ilmenite bearing cumulate layer (IBCL) introduced a gravitationally unstable situation (e.g. Shearer and Papike, 1999), likely resulting in large-scale overturn of the LMO cumulate pile (e.g. Hess and Parmentier, 1995; de Vries et al., 2010). Towards the final stages of LMO crystallisation, the residual magma ocean became progressively enriched in incompatible elements including potassium, rare earth elements, phosphorus, and high field strength elements. This reservoir enriched in incompatible trace elements subsequently provided the source for "KREEP" rich rocks (e.g. Warren, 1985; Shearer et al., 2006).

After LMO crystallisation and overturn, remelting of LMO cumulates is thought to have played a key role in the formation of mare basalts (e.g. Taylor and Jakes, 1974; Shearer and Papike, 1999; Shearer et al., 2006). While the formation process of the younger low-Ti mare basalts seems relatively straightforward, i.e. partial melting of early olivine and orthopyroxene cumulates, the formation mechanism of the older high-Ti basalts remains a matter of great debate (e.g. overviews in Shearer and Papike, 1999; Grove and Krawczynski, 2009). Both low and high-Ti basalts are saturated with olivine and orthopyroxene at similar pressures, suggesting a similar depth of origin (300-500 km, Grove and Krawczynski, 2009 and references therein). These depths are much greater than the crystallisation depths of the late-Ti rich cumulates, which crystallised at relatively shallow levels (<100 km, Snyder et al., 1992; Hess and Parmentier, 1995). Models for the formation of the high-Ti basalts have therefore suggested formation via direct melting of ilmenite-rich cumulates after overturn of the lunar mantle (e.g. Ringwood and Kesson, 1976; Hess and Parmentier, 1995; Beard et al., 1998), hybridisation of low-Ti melts by assimilation of late ilmenite- and clinopyroxene-rich cumulates (e.g. Hubbard and Minear, 1975; Wagner and Grove, 1997), or shallow level reaction and mixing of cumulates, followed by sinking of hybrid high-Ti materials (e.g. Van Orman and Grove, 2000).

Quantitative models of LMO crystallisation and its remelting rely heavily on the interpretation of the trace element composition of lunar samples (e.g. Snyder et al., 1992; Schönbächler et al., 2002; Münker 2010). To date, these models have been hampered by the lack of experimental mineral-melt partitioning data for bulk compositions, oxygen fugacities and pressure and temperature conditions relevant to LMO processes. Here, we use our new high-pressure, high-temperature orthopyroxene-melt and ilmenite-melt partitioning data obtained at LMO-relevant conditions (van Kan Parker et al., submitted MS; accepted MS), to construct quantitative forward models of the evolution of high field strength element (HFSE, Zr, Nb, Hf, Ta, Th, U) and rare earth element (REE: Nd, Sm, Lu) concentrations during crystallisation and subsequent remelting of the LMO.

2. METHODS

We evaluated two end-member LMO trace element starting compositions (Table 1): 1) a starting composition equivalent to that of the Bulk Silicate Earth (BSE) and 2) a starting composition with trace element concentrations equal to 5 x C1 chondrite values, similar to Snyder et al. (1992), but using updated C1 chondrite values from Lodders (2003). Snyder et al. (1992) chose the trace element enriched model assuming that the Moon, prior to LMO crystallisation, underwent an earlier event of differentiation, during which olivine crystallised (e.g. Taylor, 1982; Jones and Delano, 1989), e.g. 20% of the total Moon. This early event of crystallisation of olivine would have resulted in a relative increase in incompatible trace elements in the remaining LMO as opposed to the BSE, caused by the extremely low partition coefficients of olivine.

As mentioned by Elardo and Draper (2009) and Tronche and van Westrenen

Table 1. Trace element composition of the initial LMO, considering a) BSE values (McDonough, 2002) and b) 5x CI values (Lodders, 2003). Resulting trace element ratios discussed in the text are also shown.

	BSE	***5x C1 chondrite***
Nd	0.84	2.285
Sm	0.27	0.725
Lu	0.046	0.1185
Zr	7.1	19.8
Nb	0.44	1.325
Hf	0.19	0.575
Ta	0.025	0.072
Th	0.055	0.1545
U	0.015	0.042
Zr/Hf	37.4	34.4
Nb/Ta	17.6	18.4
Sm/Nd	0.32	0.32
Lu/Hf	0.24	0.21

(2009), a full experimental evaluation of the detailed crystallisation sequence during lunar magma ocean crystallisation is lacking at present. Crystallisation sequences and modes were therefore taken from the calculations of Snyder et al. (1992), based on the olivine-plagioclase-silica ternary phase diagram at 6 kbars of Longhi (1981). The first stage is characterised by olivine crystallisation, up to 40% of total LMO solidification, and is followed by orthopyroxene crystallisation, up to 78% of LMO solidification. During these first two stages, equilibrium crystallisation is assumed to have been dominant. The crystallisation of the remaining LMO is thought to have been dominated by fractional crystallisation, starting with plagioclase + olivine and pigeonite, up to 86% of LMO solidification, followed by pigeonite + clinopyroxene and plagioclase, up to 95% of LMO solidification and finally pigeonite + clinopyroxene + plagioclase and ilmenite, up to 99.5% of LMO solidification.

Mineral-melt partition coefficients for the relevant mineral phases are listed in Table 2. These partition coefficients were chosen from studies using anhydrous starting compositions, at similar experimental pressure-temperature conditions and oxygen fugacities. Only experiments using graphite-lined Pt or Mo foil sample capsules were used, such that the oxygen fugacity was close to the IW buffer, which is thought to be similar to that of the lunar interior.

As mentioned above, for orthopyroxene (Opx) and ilmenite (Ilm), our new partitioning data were used (van Kan Parker et al., submitted MS; accepted MS). Experiments in these studies were specifically designed to be suitable for the type of modelling attempted here. We also tested crystallising armalcolite as the crystallising Ti-rich mineral phase instead of ilmenite (e.g. Thacker et al., 2009), which has no obvious effect on the outcome of any of our models. This is because the partition coefficients for both armalcolite and ilmenite are very similar (van Kan Parker et al., submitted MS).

Table 2. Mineral melt partition coefficients used for the calculations in this study.

	Ol[a]	Opx[b]	Cpx[a]	Plag[c]	Ilm[d]	Arm[d]
REE						
Nd	0.00021	0.0045	0.273	0.0223	**0.00019**	**0.000011**
Sm	0.00086	0.0084	0.459	0.0116	**0.00095**	**0.000093**
Lu	0.041	0.052	0.74	**0.0018**	0.079	0.049
HFSE						
Zr	0.000064	0.0037	0.18	0.0051	0.23	0.58
Nb	0.0001*	0.0018	0.012	0.0009	0.52	0.68
Hf	0.013	0.0086	0.37	0.001	0.33	0.83
Ta	0.0006*	0.0013	0.035	0.00095	0.83	0.99
Th	0.000015	0.0015	0.021	0.00023	0.0021	0.007
U	0.00021	0.0016	0.018	0.00017	0.005	0.011

[a]McDade et al. (2003b), [a*]from MPY-90 experiment, [a*]from Tinaquillo Lherzolite experiment
[b]van Kan Parker et al. (accepted MS), [c]Tepley et al. (2010), [d]van Kan Parker et al. (submitted MS). *Note: Values in bold were fitted using the lattice strain model when partition coefficients were not available.*

For the other minerals involved in LMO crystallisation, we used previously published partition coefficients from McDade et al. (2003b) for olivine (Ol) and clinopyroxene (Cpx) and Tepley et al. (2010) for plagioclase (Plag). Plagioclase is the only mineral for which no comprehensive data set at high *P* is available. In our model, we assume that pigeonite crystallisation can be modelled using the same partition coefficients as used for clinopyroxene.

Early model attempts assumed various proportions of trapped instantaneous liquids (TRL) during LMO crystallisation as well as entrainment of minor plagioclase into late-stage cumulates by incomplete segregation (e.g. Snyder et al., 1992; Schönbächler et al., 2002; Münker, 2010) in order to explain the REE patterns and Al budget of lunar rocks, respectively. Additionally entrainment of plagioclase can account for the size of the negative Eu anomaly observed in the lunar basalts (Snyder et al., 1992). In the current model, TRL percentages between 1 and 3 wt% were considered within every cumulate package. As in previous studies (e.g. Snyder et al., 1992; Schönbächler et al., 2002; Münker, 2010), we assumed that the TRL trace element budgets are fully incorporated into the cumulate package in which they were trapped before any partial remelting of the cumulates. We also modelled the entrainment of 3 wt% plagioclase by assuming that of all crystallising plagioclase 3 wt% was mixed with sinking cumulates.

After full LMO crystallisation, we model the trace element evolution of partial melts of cumulate layers in the aftermath of large-scale mantle overturn. For our calculations we assumed fractional melting of the early Ol and Opx cumulates, followed by partial dissolution of sections of overlying material.

3. RESULTS AND DISCUSSION

Evolution of trace elements in LMO cumulates and residual liquids

Fig. 1 shows the evolution of trace element concentrations in the residual LMO liquid during progressive LMO crystallisation, for both bulk silicate earth (BSE) and 5*CI chondrite starting concentrations (Table 1). A first observation is that the predicted pattern of the latest drags of residual LMO HFSE and REE concentrations follows the measured composition of KREEP-rich rocks quite closely. From Fig. 1a we also note, that when starting with BSE starting concentrations, the LMO at 99.5% crystallisation is insufficiently enriched in trace elements to be able to explain the composition of KREEP-rich rocks. A higher percentage, i.e. >99.5% of crystallisation would be required to be able to explain the trace element composition of KREEP rich rocks.

As KREEP-rich rocks are diluted with respect to the so-called urKREEP reservoir that formed from late stage LMO crystallisation, trace element concentrations of the residual LMO need to clearly exceed those of the actual KREEP rich rocks (e.g. Warren, 1985; Shearer et al., 2006). It is therefore likely that the initial LMO trace element

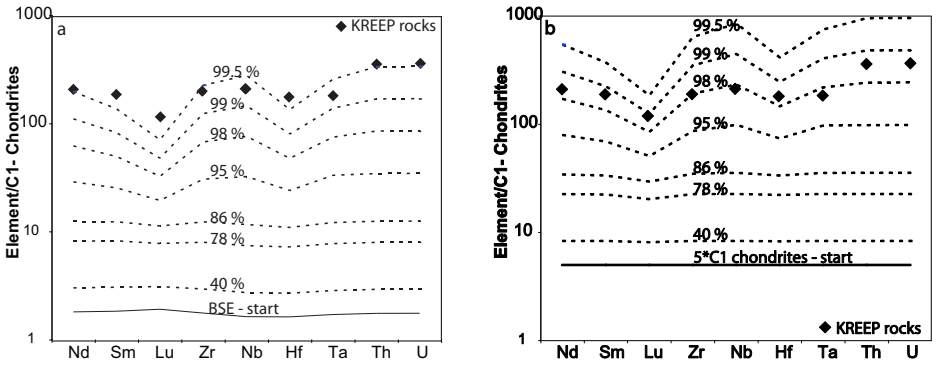

Figure 1. Evolution of selected trace element concentrations in the residual liquid upon progressive LMO crystallisation, assuming **a**) BSE starting composition and **b**) 5*CI chondrite starting values (starting concentrations shown in Table 1). Concentrations are normalised to C1 chondrite values of Lodders (2003). Percentages indicate total amount of crystallisation. Diamonds indicate composition of KREEP rich rocks (Ma and Schmitt, 1980; Neal and Kramer, 2003; Münker, 2010, and NASA lunar compendium, http://www.lpi.usra.edu/lunar/samples/).

concentrations were higher than those found in the BSE. The second scenario (Fig. 1b), assuming a 5*CI chondrite starting composition (Snyder et al., 1992), is able to explain the concentrations found in KREEP-rich rocks from ~99% of total LMO crystallisation. We use this composition as a starting point of our further calculations.

In Fig. 2, the HFSE and REE evolution of the crystallised LMO cumulates is shown. In Fig. 2a, the trace element concentrations in the crystallising cumulate pile are shown, without considering a trapped liquid (TRL) or entrainment of plagioclase. In this model, mineral-melt segregation was perfect throughout, and all formed plagioclase floated upward to form the anorthositic crust. In Fig. 2b and 2c the effects of adding 1 and 3 wt% respectively of instantaneous TRL in every cumulate layer are shown, in addition to the effect of 3 wt% total plagioclase entrainment in the plagioclase bearing cumulates.

The effect of 3 wt% plagioclase entrainment is minimal for the studied trace elements. In all cumulate packages in which plagioclase is formed, trace element concentrations decrease by ≤ 3.3% if some plagioclase is retained, due to the low concentrations of HFSE in plagioclase. In contrast, the effect of TRL incorporation is much more pronounced. When comparing Fig. 2a-c we see that entrainment of 1wt% TRL in the olivine cumulate layer leads to increases in trace element concentrations of between 1 and 3 orders of magnitude. This is related to the extremely low olivine-melt partition coefficients for the studied elements (Table 2) resulting in low trace element concentrations in the crystallising olivine cumulate. Adding a minor amount of the remaining, evolving residual liquid, which has relative high trace element concentrations, thus drastically increases the total concentrations within the olivine cumulate.

For the second, orthopyroxene cumulate layer, incorporation of 1 wt% of TRL results in an increase of about one order of magnitude for most elements (Fig. 2a versus 2b). Upon progressive crystallisation, the effect of TRL incorporation decreases for the

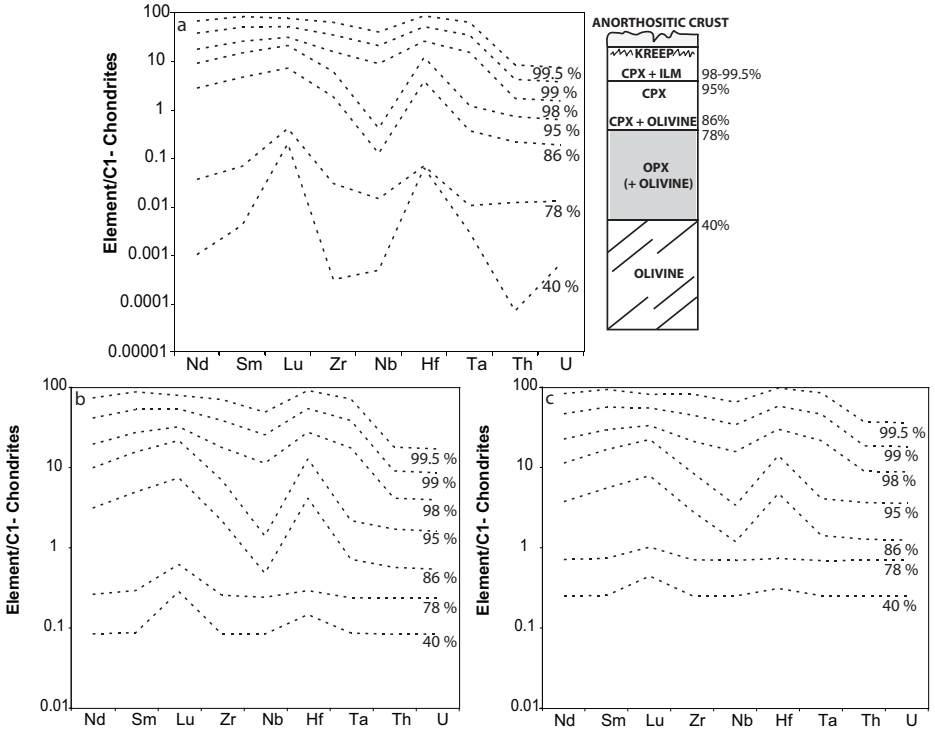

Figure 2. Trace element evolution of cumulate layers upon progressive LMO crystallisation. As reference the corresponding crystallised cumulate pile is shown (inset on right hand side), percentages correspond to the total amount of LMO crystallised at that point. The model in **a**) considers no trapped liquids are present, and all plagioclase floated upward to form the anorthositic crust. The model in **b**) assumes 1wt% of instantaneous trapped liquid in every cumulate layer as well as 3wt% of total plagioclase entrainment in the plagioclase bearing cumulates. The model in **c**) assumes 3wt% of instantaneous trapped liquid in every cumulate layer and 3wt% of total plagioclase entrainment in the plagioclase bearing cumulates.

later formed cumulates, due to the larger partition coefficients for elements in the crystallising phases, as well as the increasing trace element concentrations in the residual LMO. Increasing the percentage of entrained TRL from 1 to 3 wt% does not have a large effect on absolute trace element concentrations in the different cumulate layers (Fig. 2b versus 2c), but as discussed below, the effect on trace element ratios is more pronounced.

It should be noted that the concentrations of trace elements in the remaining liquid and cumulates shown in Fig. 1 and 2 are heavily dependent on the chosen LMO crystallisation sequence. For example, if ilmenite starts crystallising earlier, e.g. at 90% (overview in Shearer and Papike, 1999) compared to the 95% used in our model, the abundances of the HFSE in particular would be 1-6% lower in the residual liquid. This is due to the relatively high ilmenite-melt HFSE partition coefficients compared to the values for plagioclase-melt and clinopyroxene-melt partitioning.

Fig. 3 shows the predicted values of key trace element ratios (Nb/Ta, Zr/Hf, Lu/Hf and Sm/Nd) for several LMO cumulate layers and the residual LMO liquid, in comparison with values observed in lunar volcanic rocks including low-Ti, high-Ti and KREEP basalts. The assumed starting LMO composition has chondritic ratios for all four element pairs

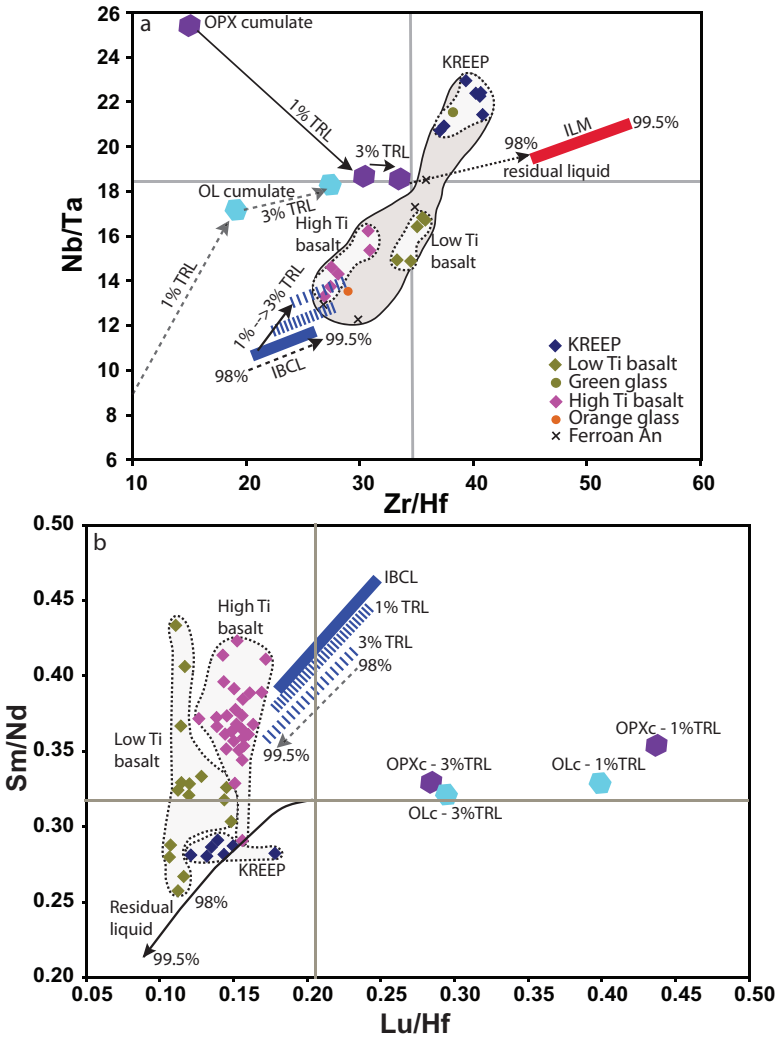

Figure 3. a) Predicted Nb/Ta versus Zr/Hf ratios in selected cumulate layers and the residual LMO liquid, compared to measured compositions of lunar volcanic rocks taken from the compilation of Münker (2010). The locations of Opx and ilmenite bearing cumulate layer (IBCL) are shown assuming no plagioclase entrainment or TRL. The corresponding Ol cumulate plots off the graph at Nb/Ta and Zr/Hf ratios of 3.1 and 0.2 respectively. The effects of 3wt% PLAG entrainment plus 1 to 3wt% TRL are indicated with arrows. **b)** Predicted Lu/Hf versus Sm/Nd ratios in selected cumulate layers and the residual LMO liquid, compared to measured compositions of lunar volcanic rocks taken from Warner et al. (1979), Ryder (2001) and Münker (2010). The evolution of the residual liquid magma ocean and the IBCL is shown from 98 to 99.5% of total LMO crystallisation, with and without 1 and 3wt% TRL and PLAG entrainment. OL and OPX cumulates with 1 and 3wt% TRL and PLAG entrainment are plotted. OL and OPX cumulates without TRL plot off the graph (OL: Lu/Hf = 0.7, Sm/Nd = 1.2; OPX: Lu/Hf = 1.2, Sm/Nd = 0.6).

(Table 1). For the residual liquid, Nb/Ta and Zr/Hf ratios become increasingly superchondritic upon crystallisation, while Sm/Nd and Lu/Hf ratios become increasingly subchondritic. Up to 78% of crystallisation, residual magma element ratios remain close to chondritic, e.g. Nb/Ta = 35.0 and Zr/Hf = 18.4 and Sm/Nd = 0.32 and Lu/Hf = 0.19. Upon further LMO crystallisation ratios deviate increasingly from chondritic starting values and change most dramatically from ≥ 95% of crystallisation. To illustrate this, Fig. 3 shows data from 98 to 99.5% crystallisation.

The evolution of the cumulates directly reflects the partition coefficients for the crystallising mineral assemblages. All cumulates formed show trace element ratios that deviate significantly from chondritic. In both Fig. 3a and 3b only the early, Ol and Opx, and late IBCL are shown, as are the effects of adding 1 and 3 wt% TRL. The Ol cumulate, with and without TRL, shows subchondritic Nb/Ta and Zr/Hf values but superchondritic Sm/Nd and Lu/Hf values. The Opx cumulate, with and without TRL, shows superchondritic Nb/Ta, Sm/Nd and Lu/Hf values but subchondritic Zr/Hf values. Finally the IBCL, with or without TRL, shows subchondritic Nb/Ta and Zr/Hf values. Sm/Nd and Lu/Hf ratios vary from superchondritic at 98% of total LMO crystallisation to subchondritic for Lu/Hf at 99.5% of LMO crystallisation.

Explaining the trace element signature of lunar mare basalts

Trace element ratios of lunar volcanic rocks differ significantly from ratios in the cumulates produced during LMO crystallisation, and from chondritic ratios (Fig. 3). KREEP basalts are characterised by superchondritic Nb/Ta and Zr/Hf ratios while their Sm/Nd and Lu/Hf ratios are subchondritic. The high-Ti basalts are characterised by subchondritic Nb/Ta, Zr/Hf, and Lu/Hf ratios, while their Sm/Nd ratios are on average superchondritic. Low-Ti basalts have Zr/Hf and Sm/Nd that average around subchondritic values, while their Nb/Ta and Lu/Hf ratios are subchondritic. Based on these measurements, Münker et al. (2003) and Münker (2010) concluded that the bulk Moon was subchondritic in Nb/Ta (Nb/Ta = 17.0).

The Apollo samples show older ages for the high-Ti basalts, 3.6-3.9 Ga, compared to the low-Ti-basalts, 3.16-3.4 Ga (Nyquist and Shih, 1992; Snyder et al., 2000). In the forthcoming discussion we therefore first discuss the formation of the high-Ti mare basalts. In Fig. 4a, 4b and 4c we test whether their observed trace element ratios can be explained by dissolution of late-formed Cpx and/or Ilm cumulate into 10% partial melts of the early Ol or Opx cumulates, as previously proposed (e.g. Wagner and Grove, 1997; Van Orman and Grove, 2000). For the trace element composition of Cpx and Ilm we assumed they continued crystallising up to 99% of total LMO crystallisation. In Figures 4a and 4b solid lines are mixing lines between partial melts from the early cumulates (Ol in Fig. 4a, Opx in Fig. 4b), both containing 1w t% TRL, while the dotted lines do not consider a TRL component.

Similar to Münker (2010) we tested the effect of dissolution of various proportions of Cpx and Ilm into the partial melts. We considered weight ratios of 2:1 (Van Orman and

Grove, 2000) and 1:3 (Wagner and Grove, 1997) and also the case in which the partial melts from the early cumulates dissolve Ilm only. The lines all start at 2 wt% of late cumulate dissolution, and end (at the arrowheads) at 20 wt% dissolution (Fig. 4a).

None of the mixing lines that consider dissolution in partial melts from an early Ol cumulate (Fig. 4a) without or with 1 wt% TRL, can explain the observed Nb/Ta and Zr/Hf ratios in the high-Ti basalts. Incorporating 3 wt% TRL would displace calculated ratios as indicated by the arced arrow.

The mixing lines involving melts from Opx cumulate with 1 wt% TRL all (partially) fall in the high-Ti field (Fig. 4b). Including a 3 wt% TRL would displace them such that only the models assuming Cpx:Ilm dissolution in the ratio 2:1 would lead to HFSE ratios that coincide with the high-Ti basalt field. Changing the percentage of TRL component increases the range of acceptable models for high-Ti basalt formation significantly. Including 3 wt% TRL enables the formation of the high-Ti basalts by mixing various proportions of Cpx and/or Ilm with partial melts from pure Ol cumulates.

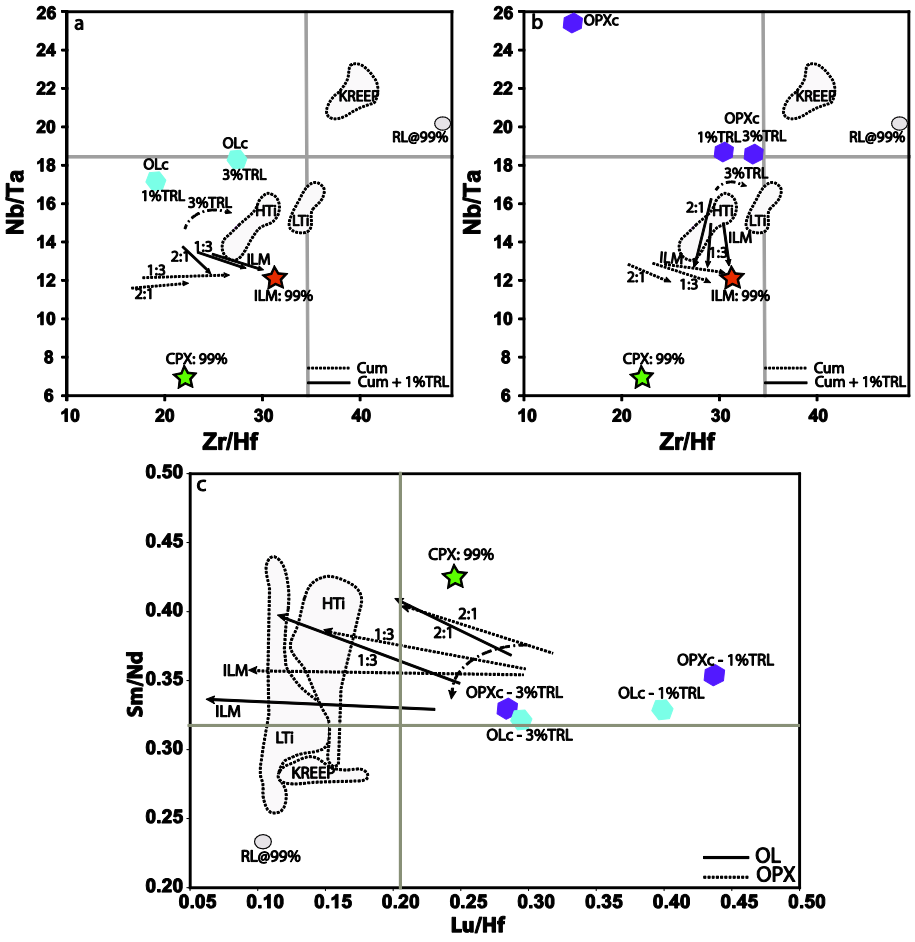

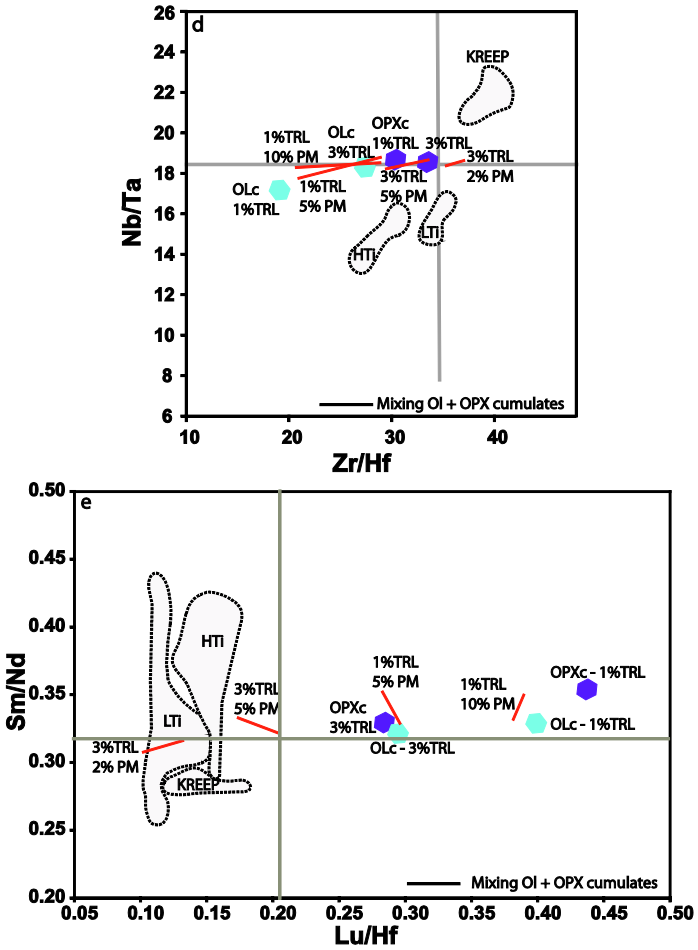

Figure 4. Illustration of the calculated trace element composition of mixtures between a 10% partially molten OL **a**), OPX **b**) or OL and OPX **c**) cumulate and CPX plus ILM (considered ratios are 2:1 and 1:3) or ILM only. Mixing proportions are 98%-80% for the partially molten OL or OPX cumulate and 2-20% of the later cumulates, Trace element signatures of CPX and ILM were calculated assuming they crystallise up to 99% of total LMO crystallisation and are shown for reference. In a) and b) the effects of mixing on Nb/Ta and Zr/Hf ratios are shown and in **c**) the effect of mixing on the Lu/Hf and Sm/Nd ratios are given. No TRL component was considered (see text). Note the 1:3 line for the Ol cumulate + TRL overlaps with the ILM only mixing line in **a**). Abbreviations are HTi and LTi for high and low-Ti basalts respectively, and RL@99% stands for the residual liquid at 99% of crystallisation. Note the 99% ILM composition is off scale in (c) at Lu/Hf = 0.03 and Sm/Nd = 1.3 **4d**) and **e**)**.** The calculated trace element composition of mixtures between partial (2-10%) melts of OL and OPX cumulates. Mixing proportions considered are 10-90% OL **d**) shows the Nb/Ta and Zr/Hf ratios while **e**) shows the Lu/Hf and Sm/Nd ratios.

Further constraints on the boundary conditions of high-Ti basalt formation are provided by Sm/Nd and Lu/Hf systematics (Fig. 4c). Since from Fig. 4a and 4b it is clear that a TRL component is essential to explain the observed trace element ratios in the high-Ti basalts, we did not consider the scenario in which no TRL would be present in this case (Fig. 4c).

Fig. 4c shows that mixing of a partial melt from Ol or Opx cumulates including 1 wt% TRL, with Cpx plus Ilm in a ratio of 2:1 can not explain the HFSE/REE signature of the high-Ti basalts: Lu/Hf values are too high (consistent with van Kan Parker et al., accepted MS). Mixing of a partially molten Ol or Opx cumulate with Cpx plus Ilm in a ratio of 1:3 or with Ilm only can reproduce the Sm/Nd and Lu/Hf values of the high-Ti basalts. When considering mixtures of Ol or Opx cumulate melts with 3 wt% TRL, both Sm/Nd and Lu/Hf ratios are displaced to lower Lu/Hf ratios specifically, as indicated by the arced arrow. However, mixing the early cumulates with a mix of 2:1 Cpx and Ilm would still not yield the concentrations observed in the high-Ti basalts.

In summary, the combined Nb/Ta, Zr/Hf, Lu/Hf and Sm/Nd systematics of high-Ti basalts are consistent with the dissolution of either pure ilmenite, or Cpx:Ilm in an approximate proportion of 1:3, into partial melts of early LMO cumulates, consistent with the model of Wagner and Grove (1997). We note that our models are able to reproduce the subchondritic Nb/Ta and Zr/Hf ratios of the high-Ti basalts assuming chondritic starting ratios for both element pairs, and that a subchondritic bulk Moon with Nb/Ta = 17.0 (Münker et al., 2003; Münker, 2010) is not required to explain the composition of the high-Ti basalts. If the initial Nb/Ta ratio is set to 17.0, similar to the approach of Münker et al. (2003) and Münker (2010), rather than a chondritic value of 18.4, the mixing lines shown in Fig. 4a and 4b would be displaced to lower values, and hence dissolution of Cpx and/or Ilm in partial melts of the Opx cumulates would not be able to explain the Nb/Ta signature of the high-Ti basalts.

To further constrain our model quantitatively it is important to constrain independently the exact proportions in which melts from the Ol and Opx cumulates mix, since here only melts from either pure Ol or pure Opx cumulate were considered. We note that although ratios can be explained very well with our forward model, absolute concentrations are all relatively low compared to measured concentrations. Adding a minor amount of KREEP component to our modelled compositions (as proposed by e.g. Münker 2010) would increase Nb/Ta and Zr/Hf ratios while decreasing Sm/Nd and Lu/Hf ratios (Fig. 4a, 4b and 4c), additionally absolute concentrations of the high-Ti basalts would increase. Additionally, late stage-fractionation effects, currently not incorporated in our model, would also increase absolute concentrations (e.g. van Kan Parker et al., submitted MS).

In Fig. 4d and 4e we show our attempts at reproducing the HFSE and REE characteristics of the younger, low-Ti mare basalts. These are generally believed to be relatively simple partial melts of the early Ol and Opx bearing cumulates (e.g. overview in Shearer and Papike, 1999). In our forward models we assess the effect of 2 to 10% partial melting of the Ol and Opx cumulates, including 1 to 3 wt% TRL, and mixing these two partial melts in varying proportions (10-90 wt%). Fig. 4d and 4e show that none of the scenarios in which we partially melt the Ol and Opx cumulate by >5% can explain any of the observed Nb/Ta and Zr/Hf or Sm/Nd and Lu/Hf ratios. The scenario in which we

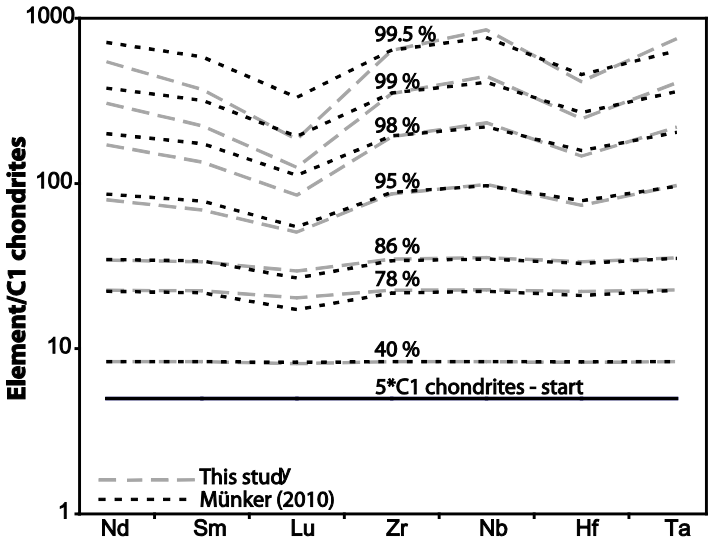

Figure 5. The effect of using *D* values in this study versus *D* values from the recent study of Münker (2010) on the trace element evolution of the crystallising LMO.

considered a 2% partially molten Ol and Opx cumulate with a 3 wt% TRL, can explain the Sm/Nd and Lu/Hf ratios (Fig. 4e), and its modelled Zr/Hf ratios are also in the right order, however the Nb/Ta ratios (Fig. 4d) are much higher than observed in the low-Ti basalts.

Assuming subchondritic Nb/Ta ratio of 17.0 for the initial LMO, as suggested by Münker (2010), would displace the Nb/Ta mixing trends to lower Nb/Ta ratios. Hence, the mixing line closest to the low-Ti field (2% partially molten Ol and Opx cumulate, including 3 wt% TRL) would be lowered by ~1 unit, but still fall above the low-Ti basalt field. We conclude that explaining the trace element signature ratios of the low-Ti basalts is not straightforward when considering multiple elemental ratios. Dissolution of olivine (without residual liquid component) or later stage cumulate possessing subchondritic Nb/Ta values seems to be required.

Comparing D values

Fig. 5 illustrates the importance of using appropriate partition coefficients in this type of lunar interior evolution modelling. It shows a comparison between the forward model constructed using the *D* values used in this study and the model constructed using the *D* values used in the recent study of Münker (2010). The difference in *D* values is most pronounced for Lu. The much lower *D* for Opx and higher *D* for Ilm used in this study result in initially higher and lower trace element concentrations during formation of the IBCL respectively. In addition, the much lower ilmenite-melt partition coefficients for Ta and Hf used in this study result in much lower absolute concentrations of these elements in ilmenite and higher concentrations in the residual LMO. For Ta this is clearly illustrated in

Fig. 5, while for Hf, reverse case seems to hold. The lower Hf values in our residual liquid compared to Münker (2010) are caused by the fact we did not take the separate contributions of Cpx and pigeonite into account, but assumed all to be clinopyroxene, since currently there are no partition coefficients that describe the partitioning behaviour of lunar pigeonite.

5. CONCLUSIONS

Quantitative forward models of the evolution of high field strength element (HFSE, Zr, Nb, Hf, Ta, Th, U) and rare earth element (REE: Nd, Sm, Lu) concentrations during crystallisation and subsequent remelting of the Lunar Magma Ocean (LMO) show that to explain the trace element concentrations observed in the KREEP rich rocks, the initial LMO was likely significantly enriched with respect to the BSE.

HFSE and REE ratios observed in the high-Ti mare basalts are consistent with partial melting of early Ol and Opx cumulates followed by dissolution of late Cpx plus Ilm in a ratio of 1:3, or mixing with Ilm only. For the low-Ti basalts the Zr/Hf, Sm/Nd and Lu/Hf ratios are best explained by a mix of 2% partially molten Ol and Opx cumulates containing a 3 wt% TRL component. However, Nb/Ta ratios in this case are elevated with respect to the measured ratios measured in the low-Ti basalts. Dissolution of a mineral or late stage cumulate possessing subchondritic Nb/Ta ratios seems required. Our models show that the subchondritic Nb/Ta ratios in lunar samples can be reproduced from an initial lunar magma ocean with chondritic Nb/Ta ratio, obviating the need for a subchondritic Nb/Ta bulk Moon.